Origin of marine barite deposits: Sr and S isotope characterization

Adina Paytan
Sarah Mearon
Department of Geological and Environmental Sciences, Stanford University, Stanford, California 94305-2115, USA
Kim Cobb
Miriam Kastner
Scripps Institution of Oceanography, La Jolla, California 92093-0212, USA

ABSTRACT

Barite can precipitate in microenvironments in the water column (marine barite), from supersaturated pore fluids at the oxic-anoxic boundary within marine sediments and where Ba-rich pore fluids are expelled and come into contact with sulfate-rich seawater (diagenetic barite), or from hydrothermal solutions (hydrothermal barite). Barite is relatively resistant to alteration after burial and has been used in paleoceanographic studies to reconstruct seawater chemistry and productivity through time. For such applications it is very important to determine the origin of the barite used, because both diagenetic and hydrothermal barite deposits may not accurately record the open-ocean contemporaneous seawater chemistry and productivity. We show here that it is possible to distinguish between the different types of barite by using Sr and S isotopes along with crystal morphology and size characteristics.

Keywords: barite, sulfur isotopes, strontium isotopes, paleoceanography.

INTRODUCTION

Barite in marine sediments is frequently used as a paleoproductivity proxy (Schmitz, 1987; Dymond et al., 1992; Gingele and Dahmke, 1994; Paytan et al., 1996a; Dean et al., 1997) as well as to reconstruct the seawater Sr isotope curve (Paytan et al., 1993; Martin et al., 1995), to determine the S isotope ratio of marine sulfate (Cecile et al., 1983; Goodfellow and Jonasson, 1984; Strauss, 1997; Paytan et al., 1998), and to characterize Holocene sedimentation rates by using excess ^{226}Ra decay (Paytan et al., 1996b; van Beek and Reyss, 2001; van Beek et al., 2002). In all these applications it is assumed that the barite crystals analyzed precipitated directly from seawater and thus recorded contemporaneous seawater productivity and chemistry. Barite microcrystals have been observed in the water column (Dehairs et al., 1980; Bishop, 1988), and there are indications that barite precipitates inorganically directly from seawater in microenvironments containing decaying organic matter and other biogenic remains (Bishop, 1988; Dehairs et al., 1990; Ganeshram and Francois, 2002). This authigenic marine barite (as defined here) precipitates as small crystals or aggregates, ranging in size from 0.5 to 5 μm (Bishop, 1988; Dehairs et al., 1980; Paytan et al., 1993).

Barite may also precipitate in association with submarine hydrothermal activity (hydrothermal barite) (Zierenberg et al., 1984; Lonsdale and Becker, 1985; Feely et al., 1987, 1990; Hannington and Scott, 1988; Peter and Scott, 1988; Kusakabe et al., 1990; Moore and Stakes, 1990) as well as diagenetically at the oxic-anoxic boundary within sediments in association with sulfate-reducing conditions (Bolze et al., 1973; Dean and Schreiber, 1977; Brumsack and Gieskes, 1983; Cecile et al., 1983; Breheret and Brumsack, 2000) or when Ba-rich fluids from seeps or along fractures are expelled into seawater (diagenetic barite) (Lonsdale, 1979; Dia et al., 1993; Torres et al., 1996a; Aquilina et al., 1997; Naehr et al., 2000). These nonbiogenic barite deposits do not necessarily reflect the contemporaneous seawater conditions (chemistry or productivity) and are therefore unsuitable for paleoceanographic studies.

Criteria to distinguish between barite crystals that form via those distinct pathways are therefore required in order to utilize this phase for paleoceanographic studies (Church, 1979). A combination of S and Sr isotope analyses and crystal-morphology characterization is suggested here to provide an indicator of the depositional environment of a given barite. Sr and/or S isotope analyses have been previously applied to describe mechanisms and conditions of barite formation; however, all previous studies were restricted to a single deposit or location (Dean and Schreiber, 1977; Hannington and Scott, 1988; Kusakabe et al., 1990; Torres et al., 1996b; Aquilina et al., 1997; Fu and Aharon, 1997; Aharon and Fu, 2000; Naehr et al., 2000; Breheret and Brumsack, 2000). Here we compare the isotope systematics and mineral-habit characteristics of a wide range of barite deposits and establish criteria to distinguish between different modes of barite formation.

ANALYTICAL METHODS

Barite was separated from other minerals in the samples by a sequential leaching procedure (Paytan et al., 1993). All samples were examined for purity by X-ray diffraction (XRD) and scanning electron microscopy (SEM) with energy-dispersive spectrometry (EDS), and only samples that contained >95% barite were used. S isotope analyses were done by continuous-flow mass spectrometry using a Carlo Erba NA 1500 elemental analyzer connected to a Micromass Isoprime mass spectrometer. Samples of 4–8 mg were introduced in tin boats with ~5 mg vanadium pentoxide mixed in with each sample. A commercial tank of SO_2 was used as a reference gas for $\delta^{34}S$ measurements, and results are reported relative to the Canyon Diablo troilite standard, with a standard deviation (2σ) of ±0.3‰. Barite samples were dissolved for Sr isotope analysis by using a resin chelation method (Paytan et al., 1993), and the Sr fraction was separated by standard ion-exchange chromatography. Values of $^{87}Sr/^{86}Sr$ were determined on a VG-261 mass spectrometer. The external precision of the analyses is ±0.000 02. All values were normalized to an $^{86}Sr/^{88}Sr$ ratio of 0.1194. During the period of analysis, the mean $^{86}Sr/^{87}Sr$ ratio of the standard NBS 987 was 0.710 24.

RESULTS AND DISCUSSION

The S and Sr isotope ratios of barite samples collected from different oceanic environments are given in Table 1 and Figure 1. Barite

TABLE 1. Sr AND S ISOTOPE COMPOSITIONS OF MARINE BARITE SAMPLES

Sample name	$^{87}Sr/^{86}Sr$	$\delta^{34}S$ (‰)	Site and sample description*
Core tops#	0.709 175	21.1	1
Sediment traps**	0.709 170	20.9	2
JDFR##, sediment trap ER 270383	0.709 178	20.8	3
JDFR##, sediment trap ER 270388	0.706 077	21.1	3
JDFR##, Clam Bed Site, 2463-R7	0.704 460	20.7	4
JDFR***, East Wall ALV 1924-6-20	0.705 210	18.2	5
JDFR***, Casm Site ALV 2084-2A-1	0.706 251	19.5	5
JDFR***, ALV 1924-6-20	0.704 415	20.5	5
JDFR***, ALV 2945-4S2,245C	0.705 243	19.2	5
JDFR###, ALV 2254-21	0.705 162	20.9	5
JDFR###, ALV 2254-23-1	0.707 141	19.7	5
JDFR****, ALV 1461-5	0.704 512	21.0	6
JDFR****, ALV 1459-8	0.705 347	20.8	6
JDFR, Southern Site, ALV 1457	0.705 518	20.9	7
Mid-Atlantic Ridge#####, ALV 2602-3	0.705 310	21.2	8
Mid-Atlantic Ridge#####, ALV 2606-3	0.705 971	20.9	8
Mid-Atlantic Ridge#####, ALV 2604-5	0.704 432	21.0	8
Mariana backarc 1830-R-1	0.704 172	21.2	9
Mariana backarc 1831-R1-C	0.705 460	21.0	9
Mariana backarc 1831-R2	0.703 991	21.1	9
Mariana backarc 1832-R2-C	0.704 762	20.9	9
East Pacific Rise 21°N, 914-R1-A	0.704 275	20.8	10
ODP Site 765C 34-1, 57–60 cm	0.710 892	24.2	11
ODP Site 765C 34-2, 118–121 cm	0.710 817	23.7	11
Peru Margin SO 78/177	0.709 939	50.6	12
Peru Margin NP 2/34	0.711 031	32.7	12
Peru Margin SO 78/180	0.710 621	45.2	12
Baja California, Ensenada, BC-1	0.708 801	28.9	13
Baja California, Ensenada, BC-2	0.708 701	29.0	13
Baja California, Ensenada, BC-3	0.708 810	29.6	13
San Clemente Basin, 355 A	0.708 487	22.1	14
San Clemente Basin, 355 B	0.708 269	23.8	14
San Clemente Basin, 355 C	0.708 372	24.6	14
Guaymas Basin 1170-16	0.706 037	24.2	15
Guaymas Basin 1172-6	0.706 251	25.7	15
Guaymas Basin 1173-1	0.706 165	26.4	15
Guaymas Basin 1173-11	0.705 649	23.2	15
Monterey Canyon, tubeworm slump	0.708 182	26.7	N.D.
Monterey Canyon 36.6°N, 122.4°W	0.708 163	31.3	16
Monterey Canyon 36.6°N, 122.4°W	0.708 215	27.1	16
Gulf of Mexico (barite crusts)	0.708 587	28.5	17
Gulf of Mexico (barite crusts)	0.708 421	59.5	17

*References for site and sample description: 1, Paytan et al. (1993, 1998); 2, Dymond and Collier (1988); 3, Dymond and Roth (1988); 4, Moore and Stakes (1990); 5, Reyes et al. (1995); 6, Shanks and Seyfried (1987); 7, Feely et al. (1987); 8, Tivey et al. (1995); 9, Kastner et al. (1987); 10, Zierenberg et al. (1984); 11, Gradstein et al. (1990); 12, Torres et al. (1996a) and Dia et al. (1993); 13, Legg (1980); 14, Lonsdale (1979); 15, Lonsdale and Becker (1985); 16, Naehr et al. (2000); 17, Fu and Aharon (1997).
#Average value of 30 core-top samples.
**Average for 9 sediment-trap samples from the Pacific Ocean.
##Juan de Fuca Ridge (JDFR) Endeavour Segment.
***JDFR Axial Seamount.
###JDFR Middle Valley.
****JDFR South Explorer Ridge.
#####Lucky Strike.

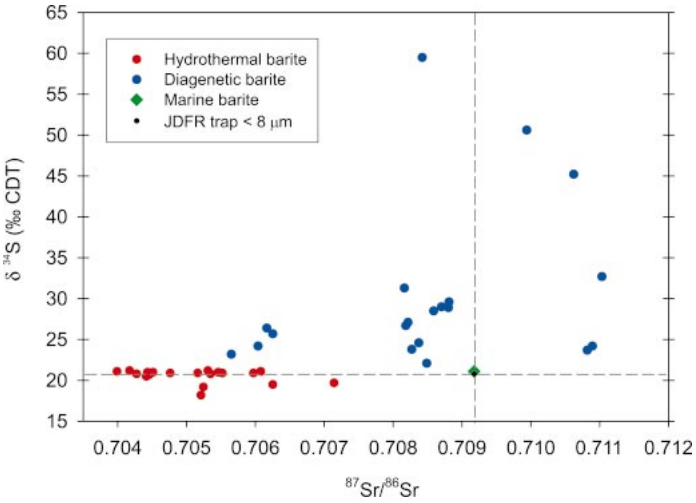

Figure 1. Plot of Sr and S isotope values for barite samples separated from different depositional environments. Green diamonds (plotted as one point)—isotope values for all core-top and sediment-trap samples (excluding Juan de Fuca Ridge [JDFR] trap) (i.e., marine barite). Blue circles—diagenetic barite samples. Red circles—hydrothermal barite samples. Black dot within diamond—barite in <8 μm fraction of Juan de Fuca Ridge trap. Dotted lines pass through present-day seawater Sr and S isotope ratios. CDT—Canyon Diablo troilite (S isotope standard).

samples cluster into three groups depending on their origin. The first very tight cluster (represented by one green diamond in Fig. 1) includes barite samples separated from core-top sediments in the Pacific, Atlantic, and Indian Oceans (30 samples) and barite crystals separated from sediment-trap samples (9 samples). These barite samples have precipitated from seawater (marine barite) and record present-day Sr (0.709 17) and S (21.1‰) isotope ratios (as determined in our laboratory).

Because the seawater Sr and S isotope ratios have not remained constant over time, the combination of Sr and S isotope ratios representing contemporaneous seawater values is different for barite separated from sediments of different ages. Accordingly, the isotope ratios for any given barite sample of known age (independently derived) should be compared to the well-known seawater Sr and S isotope curves (Burke et al., 1982; Paytan et al., 1998), and deviation from the expected contemporaneous seawater values suggests nonseawater-column origin (not marine barite).

The second category (blue circles in Fig. 1) includes barite samples with S isotope ratios higher than contemporaneous seawater values. For example, a recent massive barite deposit dredged in Baja California (Lonsdale, 1979; Table 1) has a $\delta^{34}S$ isotope value of 29.0‰ and an Sr isotope ratio of 0.708 701, clearly different from those expected for present-day seawater. These samples have precipitated from fluids that had some degree of sulfate loss due to bacterial sulfate reduction (diagenetic barite). Sulfate reduction leads to enrichment of the heavy S isotope (^{34}S) in the residual sulfate in these fluids (Harrison and Thode, 1958). Barite precipitation may occur within the sedimentary column when Ba-rich fluids (from barite dissolution by the sulfate-reduction process or from continental sources) migrate by diffusion or advection toward sulfate-rich sections in the sediment, typically at oxic-anoxic fronts (Dean and Schreiber, 1977; Kastner et al., 1990; Elderfield et al., 1990). Alternatively, barite could form at the sediment-water interface where these Ba-rich fluids are discharged through seeps or faults into sulfate-rich seawater, and barite saturation is exceeded (Torres et al., 1996a, 1996b; Naehr et al., 2000).

The Sr isotope ratio of these diagenetic barites depends on the Sr isotope ratio of the water at the site of precipitation. The Sr could have less ^{87}Sr than the Sr that is typical of contemporaneous seawater if the pore fluids have been modified by Sr from less radiogenic sources like older marine sediments or the oceanic crust (as in San Clemente Basin and Monterey Canyon); the Sr could have more ^{87}Sr relative to contemporaneous seawater if the pore-fluid Sr was derived from alteration of radiogenic terrigenous material in the sediment or meteoric water (Torres et al., 1996a; Kastner et al., 1990; Elderfield et al., 1990) (as in Peru Margin and Ocean Drilling Program Site 765C samples).

A third group is composed of barite samples (red circles in Fig. 1) characterized by Sr isotope ratios that are between the modern seawater value and the Sr isotope ratio of pure (mantle derived) hydrothermal fluids (estimated to be 0.703 50; Albarède et al., 1981). These hydrothermal barite samples precipitate from fluids influenced by hydrothermal processes. Nonradiogenic Sr as well as Ba are leached from

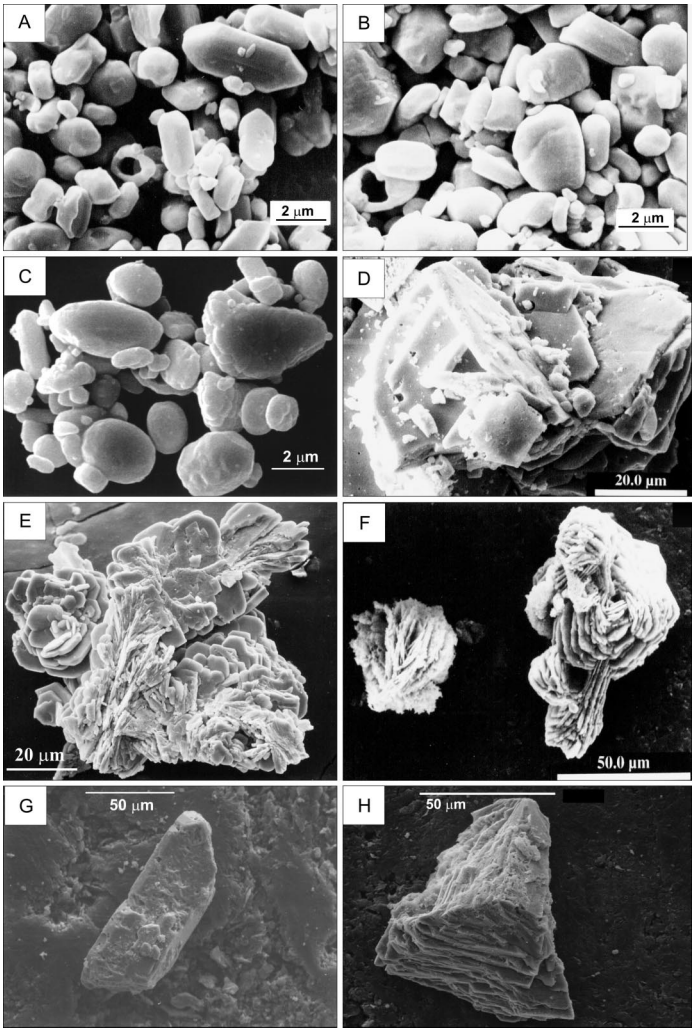

Figure 2. Scanning electron microscope images of barite crystals from different oceanic settings. A: Marine barite, core-top sediments, Pleiades expedition, core 77, 1.03°N, 119.55°W. B: Marine barite, Deep Sea Drilling Project Site 574C, 29.1 Ma. C: Marine barite, sediment trap, <8 μm fraction from Juan de Fuca Ridge black smoker. D: Hydrothermal barite, Mariana backarc chimney 1831-R1-C. E: Hydrothermal barite, Mid-Atlantic Ridge, chimney at Lucky Strike, ALV 2602-3. F: Hydrothermal barite, sediment trap, >8 μm fraction from Juan de Fuca Ridge black smoker. G: Diagenetic barite, Ocean Drilling Program Leg 132, Site 765C 34-1, 47–60 cm, ca. 112 Ma. H: Diagenetic barite, San Clemente Basin, sea cliff 355A.

the oceanic crust (basalt), and when the circulating fluids interact and mix with sulfate-rich seawater, barite may precipitate (Kusakabe et al., 1990). The S isotope ratio of these barite deposits is either equal to, or may be lower than, contemporaneous seawater depending on the relative fraction of sulfur of hydrothermal origin (H_2S oxidation) in the mixture (Hannington and Scott, 1988).

In samples separated from a sediment trap deployed at the base of a black-smoker plume on the Endeavour Segment of the Juan de Fuca Ridge (Dymond and Roth, 1988), two types of barite crystals were identified. About 20% of the particles were <8 μm, whereas 80% of the particles were >8 μm. The isotopic signatures of the size-separated fractions are distinct; the <8 μm fraction recorded present-day seawater S and Sr isotope values, and the >8 μm crystals fall into the hydrothermal barite cluster. Thus the respective origins of the barite crystals are indicated (see Table 1).

Barite samples collected from the Guaymas Basin may represent a combination of the two nonbiogenic formation processes (hydrothermal and diagenetic). The Ba and Sr source for these deposits originated most likely from hydrothermal solutions. However, in this sediment-covered ridge system, the fluids are expelled into marine-sediment sections where sulfate reduction takes place, depleting the pore-water sulfate from the light S isotope and resulting in barite with S isotope ratios slightly greater than seawater (Elsgaard et al., 1994).

In addition to the characteristic isotopic signatures of barite deposited in the different marine settings already described, the size and morphology of barite crystals formed by those different precipitation modes are distinct. Figure 2 shows SEM micrographs of typical barite crystals separated from the different depositional environments. Marine barite crystals precipitated in the water column and extracted from sediment-trap samples (including the <8 μm barite fraction from the Juan de Fuca Ridge black smoker) or from marine sediments that have not undergone extensive sulfate reduction are smaller than 5 μm and are typically ellipsoidal in shape (Fig. 2, A–C). Hydrothermal barite crystals are larger, 20–70 μm, and are typically precipitated as cross-cutting tabular crystals commonly forming rosettes (Fig. 2, D–F). The >8 μm barite crystals from the sediment trap above the Juan de Fuca Ridge, as expected, have morphological features typical of hydrothermal precipitates. Diagenetic barite crystals are also large (20–700 μm), flat, tabular-shaped crystals and appear as barite beds in the sedimentary column. Diagenetic barite crystals that precipitate at the sediment-water interface form mounds of highly porous barite with the layered appearance of platy crystals that form diamond-shaped clusters (Fig. 2, G–H).

CONCLUSIONS

On the basis of crystal size and morphology and the Sr and S isotope ratios of barite deposits, it is possible to distinguish between the depositional environments and thus the origin of this mineral if the age of the barite sample is independently determined. Careful examination of barite samples used for paleoceanographic studies would eliminate any questions with respect to the authenticity of marine barite origin and its fidelity in recording the seawater characteristics (productivity and/or chemistry).

ACKNOWLEDGMENTS

We thank Peter Lonsdale, Debra Stakes, Billy Moore, Martha Torres, Margaret Tivey, Richard Zierenberg, Thomas Naehr, Harmon Craig, Jack Dymond, and Bob Collier for generously sharing their barite samples or sediment-trap material with us. We thank the Repositories of the Scripps Institution of Oceanography and Oregon State University (OCE-9102881) for providing core-top samples for barite separation. Older marine barite samples were separated from Ocean Drilling Program and Deep Sea Drilling Project cores. Comments by P. van Beek greatly improved the manuscript. This work was supported by National Science Foundation grants OCE-91-16010 and EAR-96-28479.

REFERENCES CITED

Aharon, P., and Fu, B.S., 2000, Microbial sulfate reduction rates and sulfur and oxygen isotope fractionations at oil and gas seeps in deepwater Gulf of Mexico: Geochimica et Cosmochimica Acta, v. 64, p. 233–246.

Albarède, F., Michard, A., Minster, J.F., and Michard, G., 1981, Strontium-87/strontium-86 ratios in hydrothermal waters and deposits from the East Pacific Rise at 21°N: Earth and Planetary Science Letters, v. 55, p. 229–236.

Aquilina, L., Dia, A.N., Boulegue, J., Bourgois, J., and Fouiliac, A.M., 1997, Massive barite deposits in the convergent margin off Peru: Implications for fluid circulation within subduction zones: Geochimica et Cosmochimica Acta, v. 61, p. 1233–1245.

Bishop, J.K.B., 1988, The barite–opal–organic carbon association in oceanic particulate matter: Nature, v. 331, p. 341–343.

Bolze, C.E., Malone, P.G., and Smith, M.J., 1973, Microbial mobilization of barite: Chemical Geology, v. 13, p. 341–343.

Breheret, J.G., and Brumsack, H.J., 2000, Barite concretions as evidence of pauses in sedimentation in the Marnes Bleues Formation of Vocontian Basin (SE France): Sedimentary Geology, v. 130, p. 205–228.

Brumsack, H., and Gieskes, J.M., 1983, Interstitial water trace metal chemistry of laminated sediments from the Gulf of California, Mexico: Marine Chemistry, v. 14, p. 89–106.

Burke, W.H., Denison, R.E., Hetherington, E.A., Koepnick, R.B., Nelson, H.F.,

and Otto, J.B., 1982, Variation of seawater $^{87}Sr/^{86}Sr$ throughout Phanerozoic time: Geology, v. 10, p. 516–519.
Cecile, M.P., Shakur, M.A., and Krouse, H.R., 1983, The isotopic composition of western Canadian barites and the possible derivation of oceanic sulfate $\delta^{34}S$ and $\delta^{18}O$ age curves: Canadian Journal of Earth Sciences, v. 20, p. 1528–1535.
Church, T.M., 1979, Marine barite, *in* Burns, R.G., ed., Marine minerals: Washington, D.C., Mineralogical Society of America, p. 175–209.
Dean, W.E., and Schreiber, B.C., 1977, Authigenic barite, *in* Lancelot, Y., et al., Proceedings of the Deep Sea Drilling Project, Initial reports, Volume 41: Washington, D.C., U.S. Government Printing Office, p. 915–931.
Dean, W.E., Gardner, J.V., and Piper, D.A., 1997, Inorganic geochemical indicators of glacial-interglacial changes in productivity and anoxia on the California continental margin: Geochimica et Cosmochimica Acta, v. 61, p. 4507–4518.
Dehairs, F., Chesselet, R., and Jedwab, J., 1980, Discrete suspended particles of barite and the barium cycle in the open ocean: Earth and Planetary Science Letters, v. 49, p. 529–550.
Dehairs, F., Goeyens, L., Stroobants, N., Bernard, P., Goyet, C., Poisson, A., and Chesselet, R., 1990, On the suspended barite and the oxygen minimum in the Southern Ocean: Global Biogeochemical Cycles, v. 4, p. 85–102.
Dia, A.N., Aquilina, L., Boulegue, J., Bourgois, J., Suess, E., and Torres, M., 1993, Origin of fluids and related barite deposits at vent sites along the Peru convergent margin: Geology, v. 21, p. 1099–1102.
Dymond, J., and Collier, R., 1988, Biogenic particle fluxes in the equatorial Pacific: Evidence for both high and low productivity during the 1982–83 El Niño: Global Biogeochemical Cycles, v. 2, p. 129–137.
Dymond, J., and Roth, S., 1988, Plum dispersed hydrothermal particles: A time-series record of settling flux from the Endeavour Ridge using moored sensors: Geochimica et Cosmochimica Acta, v. 52, p. 2525–2536.
Dymond, J., Suess, E., and Lyle, M., 1992, Barium in deep-sea sediments: A geochemical proxy for paleoproductivity: Paleoceanography, v. 7, p. 163–181.
Elderfield, H., Kastner, M., and Martin J.B., 1990, Composition and sources of fluids in sediments of the Peru subduction zone: Journal of Geophysical Research, v. 95, p. 8819–8828.
Elsgaard, L., Isaksen, M.F., Jorgensen, B.B., Alayse, A.M., and Jannasch, H.W., 1994, Microbial sulfate reduction in deep-sea sediments at the Guaymas Basin hydrothermal vent area: Influence of temperature and substrates: Geochimica et Cosmochimica Acta, v. 58, p. 3335–3343.
Feely, R.A., Maureen, L., Massoth, G.J., Robert-Baldo, G., Lavelle, J.W., Byrne, R.H., Von-Damm, K.L., and Curl, H.C., 1987, Composition and dissolution of black smoker particulates from active vents on the Juan de Fuca Ridge: Journal of Geophysical Research, v. 92, p. 11 347–11 363.
Feely, R.A., Geiselman, E.T., Backer, E.T., and Massoth, G.J., 1990, Distribution and composition of hydrothermal plume particles from the ASHES vent field at Axial volcano, Juan de Fuca Ridge: Journal of Geophysical Research, v. 95, p. 12 855–12 873.
Fu, B., and Aharon, P., 1997, Origin and depositional model of barite deposits associated with hydrocarbon seeps on the Gulf of Mexico slope: Gulf Coast Association of Geological Societies Transactions, v. 46, p. 125–131.
Ganeshram, R., and Francois, R., 2002, New insights into the mechanism of barite formation in seawater and implications for paleoproductivity reconstruction: Eos (Transactions, American Geophysical Union), v. 83, Ocean Science Meeting Supplement, Abstract OS21L–11.
Gingele, F., and Dahmke, A., 1994, Discrete barite particles and barium as a tracer of paleoproductivity in South Atlantic sediments: Paleoceanography, v. 9, p. 151–168.
Goodfellow, W.D., and Jonasson, I.R., 1984, Ocean stagnation and ventilation defined by ^{34}S secular trends in pyrite and barite; Selwyn Basin, Yukon: Geology, v. 12, p. 583–586.
Gradstein, F.M., Ludden, J., et al., 1990, Proceedings of the Ocean Drilling Program, Initial reports, Volume 123: College Station, Texas, Ocean Drilling Program, p. 269–352.
Hannington, M.D., and Scott, R., 1988, Mineralogy and geochemistry of hydrothermal silica-sulfide-sulfate spire in the caldera of Axial Seamount, Juan de Fuca Ridge: Canadian Mineralogist, v. 26, p. 603–625.
Harrison, A.G., and Thode, H.G., 1958, Mechanism of bacterial reduction of sulfate from isotope fractionation studies: Faraday Society Transactions, v. 54, p. 84–92.
Kastner, M., Craig, H., and Sturz, A., 1987, Hydrothermal deposition in the Mariana trough: Preliminary mineralogical investigation: Eos (Transactions, American Geophysical Union), v. 68, p. 1499.
Kastner, M., Elderfield, H., Martin, J.B., Suess, E., Kvenvolden, A., and Garrison, R.E., 1990, Diagenesis and interstitial water chemistry at the Peruvian continental margins—Major constituents and strontium isotopes, *in* Suess, E., and von Huene, R., Initial reports of the Ocean Drilling Program, Volume 112 B: College Station, Texas, Ocean Drilling Program, p. 413–440.
Kusakabe, M., Mayeda, S., and Nakamura, E., 1990, S, O, and Sr isotope systematics of active vent materials from the Mariana backarc basin spreading-axis at 18°N: Earth and Planetary Science Letters, v. 100, p. 275–282.
Legg, M.R., 1980, Seismicity and tectonics of the inner continental borderland of southern California and northern Baja California, Mexico [M.S. thesis]: San Diego, University of California, 107 p.
Lonsdale, P., 1979, A deep-sea hydrothermal site on a strike-slip fault: Nature, v. 281, p. 531–534.
Lonsdale, P., and Becker, K., 1985, Hydrothermal plumes, hot springs, and conductive heat flow in the Southern Trough of Guaymas Basin: Earth and Planetary Science Letters, v. 73, p. 211–225.
Martin, E.E., Macdougall, J.D., Herbert, T.D., Paytan, A., and Kastner, M., 1995, Strontium and neodymium isotopic analyses of marine barite separates: Geochimica et Cosmochimica Acta, v. 59, p. 1353–1361.
Moore, W.S., and Stakes, D., 1990, Ages of barite-sulfide chimneys from the Mariana Trough: Earth and Planetary Science Letters, v. 100, p. 265–274.
Naehr, T.H., Stakes, D.S., and Moore, W.S., 2000, Mass wasting, ephemeral fluid flow, and barite deposition on the California continental margin: Geology, v. 28, p. 315–318.
Paytan, A., Kastner, M., Martin, E.E., Macdougall, J.D., and Herbert, T., 1993, Marine barite as a monitor of seawater strontium isotope composition: Nature, v. 366, p. 445–449.
Paytan, A., Kastner, M., and Chavez, F.P., 1996a, Glacial to interglacial fluctuations in productivity in the equatorial Pacific as indicated by marine barite: Science, v. 274, p. 1355–1357.
Paytan, A., Moore, W.S., and Kastner, M., 1996b, Sedimentation rate as determined by ^{226}Ra activity in marine barite: Geochimica et Cosmochimica Acta, v. 60, p. 4313–4319.
Paytan, A., Kastner, M., Campbell, D., and Thiemens, M.H., 1998, Sulfur isotope composition of Cenozoic seawater sulfate: Science, v. 282, p. 1459–1462.
Peter, J.M., and Scott, S.D., 1988, Mineralogy, composition, and fluid-inclusion microthermometry of seafloor hydrothermal deposits in the southern trough of Guaymas Basin, Gulf of California: Canadian Mineralogist, v. 26, p. 567–658.
Reyes, A.O., Moore, W.S., and Stakes, D.S., 1995, $^{228}Th/^{228}Ra$ ages of a barite-rich chimney from the Endeavour Segment of the Juan de Fuca Ridge; Earth and Planetary Science Letters, v. 131, p. 99–113.
Schmitz, B., 1987, Barium, equatorial high productivity, and the wandering of the Indian continent: Paleoceanography, v. 2, p. 63–77.
Shanks, W.S., III, and Seyfried, W.E., Jr., 1987, Stable isotope studies of vent fluids and chimney minerals, South Juan de Fuca Ridge: Sodium metasomatism and seawater sulfate reduction: Journal of Geophysical Research, v. 92, p. 11 387–11 399.
Strauss, H., 1997, The isotopic composition of sedimentary sulfur through time: Palaeogeography, Palaeoclimatology, Palaeoecology, v. 132, p. 97–118.
Tivey, M.K., Humphries, S.E., Thompson, G., Hannington, M.D., and Rona, P.A., 1995, Deducing patterns of fluid flow and mixing within the TAG active hydrothermal mound using mineralogical and geochemical data: Journal of Geophysical Research, v. 100, p. 12 527–12 555.
Torres, M.E., Bohrmann, G., and Suess, E., 1996a, Authigenic barites and fluxes of barium associated with fluid seeps in the Peru subduction zone: Earth and Planetary Science Letters, v. 144, p. 469–481.
Torres, M.E., Brumsack, H.J., Bohrmann, G., and Emeis, K.C., 1996b, Barite fronts in continental sediments: A new look at barium remobilization in the zone of sulfate reduction and formation of heavy barites in authigenic fronts: Chemical Geology, v. 127, p. 125–139.
van Beek, P., and Reyss, J.-L., 2001, ^{226}Ra in marine barite: New constraints on supported ^{226}Ra: Earth and Planetary Science Letters, v. 187, p. 147–161.
van Beek, P., Reyss, J.-L., Paterne, M., Gersonde, R., Rutgers van der Loeff, M., and Kuhn, G., 2002, ^{226}Ra in barite: Absolute dating of Holocene Southern Ocean sediments and reconstruction of sea-surface reservoir ages: Geology, v. 30, p. 731–734.
Zierenberg, R.A., Shanks, W.C., III, and Bischoff, J.L., 1984, Massive sulfide deposits at 21°N, East Pacific Rise: Chemical composition, stable isotopes, and phase equilibria: Geological Society of America Bulletin, v. 95, p. 922–929.

Manuscript received January 16, 2002
Revised manuscript received April 25, 2002
Manuscript accepted April 30, 2002

Printed in USA